Geochemical modelling of the effect of waste degradation processes on the long-term performance of waste forms

Erich Wieland[1]*, Georg Kosakowski[1], Barbara Lothenbach[2], Dmitrii A. Kulik[1]

[1] Paul Scherrer Institut, Laboratory for Waste Management, 5232 Villigen PSI, Switzerland

[2] Empa, Laboratory for Concrete & Construction Chemistry, 8600 Dübendorf, Switzerland

Prepared for publication in *Applied Geochemistry*

*corresponding author:

E-Mail address: erich.wieland@psi.ch

Key words: waste package, steel, organics, aggregates, degradation, modelling

Abstract

The near field of the planned deep geological repository for low- and intermediate-level radioactive waste (L/ILW) in Switzerland will consist of different waste materials with different reactivities that are conditioned in cementitious matrices. Geochemical modelling was applied to predict the temporal evolution of the chemical conditions in a cement-stabilised model waste form by simulating the degradation of the waste materials and the alteration of the cementitious matrix. The model waste form contains large amounts of metallic waste and a low amount of organic waste. The geochemical modelling considered the use of either siliceous or calcareous aggregates for fabrication of the cementitious matrix used to condition the waste form. The results show that the type of aggregates has a major effect on the temporal evolution of the chemical conditions in the waste form. The use of calcareous aggregate instead of the commonly used siliceous aggregate is expected to maintain highly alkaline conditions of the waste form over the period of concern for the L/ILW repository. The latter conditions prevent accelerated iron corrosion and, related to that, accelerated H_2 production from occurring due to the high pH. The evolution of the waste form is decisively controlled by the availability of water. In the absence of water ingress from the near field, the degradation process ceases as free water in the waste package is exhausted. In the case of saturation achieved by water ingress with time, the degradation processes continue over the entire period of concern for the L/ILW repository. The present study aims to illustrate the potential of geochemical modelling for predicting the temporal evolution of the chemical conditions of a cement-stabilised waste form.

1. Introduction

The Swiss disposal concept for low- and intermediate-level waste (L/ILW) foresees waste isolation by a multi-barrier system in a stable geologic formation (Nagra, 2002, 2016). Although the inventory of radionuclides in the L/ILW repository and the radiotoxicity associated with L/ILW are much less than those in the planned spent fuel and high-level waste repositories, the variety of waste materials with different reactivity may be of importance in conjunction with the long-term performance of the repository. The various components of the multi-barrier system of the L/ILW repository contribute to ensuring safe disposal of the waste forms for a very long period. The barriers include the waste matrix, steel drums, infill mortar, emplacement containers, the cavern backfill, the liner and the host rock. Cementitious materials will be used as encapsulants as well as backfill and construction materials. The materials will be emplaced in a manner to function as the major physical and chemical barriers to the release of radionuclides from the cementitious near field into the host rock. For safety assessment (SA) modelling it is considered that hardened cement paste of the solidifying cementitious material in waste packages and in the cavern backfill is the most important material available in the near field that is capable of retarding the migration of radionuclides. The source term for radionuclide migration from the near field into the geologic formation, which is considered the main barrier for radionuclide migration in the Swiss disposal concept, is determined by partition of radionuclides between hardened cement paste and pore solution.

Very different types of materials contribute to the inventory of a cement-based L/ILW repository, such as metallic and organic wastes, conditioned in a solidifying cementitious matrix. These materials are subjected to degradation processes and therefore, it is expected that the barrier function of the near field will alter with time due to interaction of the products from waste degradation with the solidifying cementitious material. The degradation processes include i)

(bio)chemical degradation of organic wastes and the interaction of the main degradation products, CO_2 (and it bases) with hydrated cement, ii) corrosion of the metallic waste materials and the interaction of corrosion products with hydrated cement, and iii) internal degradation of hydrated cement due to interaction of highly alkaline cement pore water with siliceous aggregate in the cementitious environment (Kosakowski et al., 2014; Huang et al., 2018). These processes account for the alteration of the cementitious materials of the engineered barrier by internal processes, which occur in addition to external processes. The latter processes are related to the infiltration of formation water, which is very low in claystone host rock due to diffusive transport across the cement-clay interface (e.g. Walton et al., 1997; De Windt et al., 2004; Gaucher et al., 2004; Marty et al., 2015).

To the best of our knowledge the effect of waste degradation on the chemical evolution of the conditions in waste packages has not yet been explored in detail, while it was noted that state-of-the-art modelling of waste container and waste package performance is required for long-term predictions in support of safety assessment (Askarieh et al., 2000; Askarieh et al., 1998; Sullivan, 2004; Small and Thompson, 2008). In a previous study (Wieland et al., 2018), it was demonstrated that the long-term evolution of the chemical conditions of cemented model waste forms can be assessed by geochemical modelling using the Gibbs Energy Minimization Selektor (GEM-Selektor) software package (Kulik et al., 2013; http://gems.web.psi.ch). A consistent set of thermodynamic data for cement phases is nowadays available that allows the initial conditions in waste packages to be modelled and conversion of the cementitious materials by the degradation of wastes to be predicted as a function of time (e.g. Lothenbach et al., 2019; https://www.empa.ch/cemdata).

The simulations reported in this study aim to demonstrate the potential of geochemical modelling to assess the effect and consequences of waste evolution, exemplarily illustrated for a model waste form and matrix. The approach provides important geochemical information (volume and

chemical composition of gas phase, solution and mineral assemblage) over the entire period of concern for the L/ILW repository, which is assumed to be 10^5 years. The approach allows the relevance of degradation processes on the evolution of the chemical conditions in waste packages to be assessed and trends in the long-term behaviour of the various waste forms to be identified. In this study, the modelling approach previously outlined by Wieland et al. (2018) was applied with the aim of addressing the effect of different types of aggregates on the temporal evolution of a decommissioning model waste form. Geochemical modelling was performed by assuming that either siliceous or calcareous aggregates are employed for fabrication of the cementitious material used for waste encapsulation. Otherwise, the same concepts and model parameters were applied as previously reported by Wieland et al. (2018). The modelling approach assumes that all materials are evenly distributed inside a waste package, i.e. homogenised in accordance with a "mixing tank" and further that transport processes are not rate-limiting. As a consequence of this, the modelling approach does not provide information on the spatially resolved evolution of the chemical conditions in a waste package and, in particular, it does not account for the effect of gas production on transport processes in the waste package. It is to be noted that gas production and transport processes could significantly affect the time scales reported in this study for the chemical evolution of the waste form. Furthermore, the observed processes cannot be up-scaled to the repository-level as the model does not account for chemical interaction of the conditioned waste matrix with the container and the surrounding cavern materials.

2. Waste form

2.1 Inventory

A potential waste form produced during decommissioning of nuclear power plants was considered for this study. The material inventory listed in Table 1 has been selected from the database for a model waste form (Nagra, 2014).

The waste materials will be stored in a concrete container, which has a total volume of 5.95 m^3, and stabilised by the solidifying cementitious material. The waste form mainly contains metallic waste, such as steel (5930 kg), cast iron (210 kg), copper (139 kg), brass (124 kg), aluminium (3.17 kg) and zinc (0.557 kg). The inventory of organic materials is comparably low, i.e. comprising small amounts of low molecular weight (LMW) organics (12.92 kg), polyvinyl chloride (PVC) (0.752 kg), and urea (4.49 kg).

Table 1: Materials present in the model waste form (Nagra, 2014).

Material	Mass (kg)	Material	Mass (kg)
Aluminium	3.17	Polyvinyl chloride (PVC)	0.752
Brass	124	Quartz sand	1950
Cement (unhydrated)	1250	Silica fume (“Micropoz”)	375
Clinoptilolite	187	Steel	5930
Copper	139	Urea	4.49
Iron (cast)	210	Water	757
LMW organics	12.92	Zinc	0.557

2.2 Materials used for fabrication of the solidifying cementitious matrix

The solidifying cementitious material is made at a water/binder (w/b) ratio of ~ 0.42 (binder materials: sulphate-resisting ordinary Portland cement (OPC), clinoptilolite, silica fume as given in Table 2) and using quartz sand as aggregate in the original formulation (Table 1).

Addition of clinoptilolite, a natural zeolite, is considered to improve Cs retention while silica fume (“Micropoz”) is added to reduce the volume of free water. According to the MIRAM 14 databases (Modellhaftes Inventar für RAdioaktive Materialien) quartz sand is used as siliceous aggregate for fabrication of the solidifying cementitious matrix (Nagra, 2014). In this study it was assumed that siliceous aggregate can be replaced by calcareous aggregate (limestone). Note that only the solidifying cementitious matrix inside the container was considered, while other concrete structures, in particular concrete of the emplacement container, were ignored.

Table 2: Materials used for fabrication of the solidifying cementitious material.

	Mass (kg)[a]	
Mix	Original	Alternative
Water	757	*757*
Binders		
- HTS cement (unhydrated)	1250	*1250*
- Silica fume ("Micropoz")[b]	375	*375*
- Clinoptilolite[b]	187	*187*
Gluconic acid (Na form)[c]	(3.12)	(3.12)
Quartz sand	1950	
Calcareous aggregate		*1950*

[a] Only the solidifying cementitious material was considered for the modelling, thus implying that the emplacement container for this waste form was not considered;

[b] Silica fume and clinoptilolite were assumed to have the same reactivity during hydration;

[c] Gluconic acid (superplasticizer) was not considered for modelling the initial conditions.

2.3 Composition of sulphate-resisting OPC

Chemical and normative phase compositions of the HTS CEM I 52.5 cement (HTS = Haute Teneur en Silice, Lafarge, France) listed in Table 3 have been taken from earlier studies (Lothenbach and Wieland, 2006; Berner, 2009). The aluminate and ferrite contents are relatively low, and the cement has been classified as sulphate-resistant. The contents of Li_2O and Rb_2O are very low and, for the sake of simplification, they were assigned to the Na_2O content.

The mineral composition of cement paste has not been reported in the MIRAM 14 databases (Nagra, 2014). This information was gained by thermodynamic modelling of cement hydration in accordance with earlier work (Lothenbach and Wieland, 2006; Berner, 2009).

2.4 Metals

Steel and cast iron are the most important metallic waste materials present in this waste form, while the inventories of aluminium, brass, copper and zinc are comparatively small. It was assumed that all steel is present as carbon steel (89.4 wt.% of steel inventory) and consists of pure iron. This is a conservative assumption as a small portion of the metallic waste will be stainless

steel (10.6 wt.% of steel inventory) (Diomidis et al., 2016). Brass is a CuZn alloy, and for modelling purposes, a Cu:Zn 1:1 stoichiometry (molar ratio) was assumed. All metals except copper were considered to be susceptible to anoxic corrosion, while no corrosion rates were available for copper (Diomidis, 2014). Hence, copper was considered to be subject to instantaneous reaction.

Table 3: Chemical and normative phase compositions of HTS CEM I 52.5 N according to Lothenbach and Wieland (2006) and Berner (2009).

Chemical Analysis	HTS (g/100 g)	Normative composition	HTS (g/100 g)
CaO[a]	66.15	Alite[d] (C_3S)	61
SiO_2	22.3	Belite[d] (C_2S)	18
Al_2O_3	2.7	Aluminate[d] (C_3A)	3.9
Fe_2O_3	1.9	Ferrite[d] (C_4AF)	5.8
MgO	0.85	CaO (free)	0.45
SrO	0.16	$CaCO_3$	3.7
BaO	0.002	Gypsum ($CaSO_4 \cdot 2H_2O$)	1.3
K_2O	0.22	Hemihydrite ($CaSO_4 \cdot 0.5H_2O$)	1.1
Na_2O[b]	0.19	Anhydrite ($CaSO_4$)	1.5
CO_2	1.6	K_2SO_4	0.14
SO_3	2.2	Na_2SO_4	0.09
LOI[c]	1.728	K_2O	0.14
		Na_2O	0.09
		MgO	0.85
		SrO	0.16
		BaO	0.002
		SO_3	0.01

[a] Reactive CaO also contains 0.45 g/100 g free lime.

[b] The amount of Na_2O also accounts for Li_2O (0.03 % =10.04 mmol/g) and Rb_2O as Li and Rb is not considered in the calculations;

[c] Loss on ignition (LOI) is not specified and considered as "inert phase" with the properties of quartz (Berner, 2009).

[d] Cement notation: C = CaO, S = SiO_2, A = Al_2O_3, F = Fe_2O_3

2.5 Organics

Low-molecular-weight organics comprise small, readily degradable molecules, such as diethanolamine, formaldehyde, gluconic acid, methanol, melamine resins, surfactants etc. For modelling purposes, the amount of urea was assigned to the inventory of LMW organics. PVC was

the only slowly degrading polymeric material present in this waste form.

3. Degradation processes

3.1 Decomposition of organic matter

For SA, two broad categories of organic wastes have been classified: a) readily degrading organic compounds, such as cellulose and LMW organics (e.g. detergents, surfactants, cement admixtures etc.) and b) slowly degrading polymeric organic materials, such as acrylic glass, bitumen, plastics, polystyrene, PVC, resins, and rubber that may be resistant to complete degradation (Wiborgh et al., 1986; Nagra, 2008). Decomposition of organic waste materials, presumably catalysed by microbes, will produce methane (CH_4) and carbon dioxide (CO_2) as follows:

LMW organics: $C_2H_4O_2 = CO_2 + CH_4$ PVC: $4\ C_2H_3Cl + 6\ H_2O = 3\ CO_2 + 5\ CH_4 + 4\ HCl$

The reaction stoichiometries have been developed on the basis of the following assumptions: 1) acetic acid (CH_3COOH) is the surrogate for LMW organics, and 2) polymeric PVC is decomposed into its monomeric component (C_2H_3Cl) (Wieland et al., 2018). Hence, organic matter is characterised in terms of the mean oxidation state of carbon and the carbon content, which were determined from the monomeric components of the polymeric materials. The oxidation state of carbon corresponds to the reduction capacity of organic matter, and determines the ratio of CH_4 to CO_2 produced during decomposition. The carbon content determines the total volume of CH_4 and CO_2 produced in the course of decomposition. Details of the material properties and implementation for modelling purposes are reported elsewhere (Wieland et al., 2018).

The degradation rates of organic matter were estimated on the basis of currently used reference gas generation rates for SA (Wiborgh et al., 1986). The reference rates per year (annum: a) were 0.07 mol kg^{-1} a^{-1} in case of the readily degrading materials (e.g. LMW organics) and 0.005 mol kg^{-1} a^{-1} in case of the slowly degrading materials (e.g. PVC). From investigations of gas generation rates of actual mixed wastes in both brine and cementitious waters it was claimed that gas generation

rates could be more than an order of magnitude lower than the above reference values (Kannen and Müller, 1999). Furthermore, the rates imply the possibility of microbial degradation of organic matter, which is limited in strongly alkaline conditions although the latter are unlikely to prevent microbial activity from occurring.

The reference gas generation rates expressed in terms of moles of gas produced per kilogram organic matter per year (mol kg^{-1} a^{-1}) can be converted into a first-order degradation kinetics of the organics (Wieland et al., 2018):

$$m(t) = m(0) \cdot e^{-k_D t} \quad \text{(mol)} \qquad (1)$$

m(0): Initial inventory of organic matter (mol)

k_D: Degradation rate constant (a^{-1})

The rate constants were estimated to be $k_D = 2.10 \cdot 10^{-3}$ a^{-1} for LMW organic matter and $k_D = 3.91 \cdot 10^{-5}$ a^{-1} for PVC (Wieland et al., 2018), respectively. The degradation rates are consistent with those used for modelling gas generation in a deep geological repository (Poller et al., 2016). Hence, LMW organics are predicted to decompose almost completely (1% residual inventory) within about 2200 years, while the decomposition of PVC is much slower, i.e. a 1% residual inventory is achieved in about $1.2 \cdot 10^5$ years (Figure 1).

The proposed model for the decomposition of readily degrading organic matter is supported by experimental evidence. The rate constant of hydrolysis of reactive cellulose was estimated to be $1.35 \cdot 10^{-3}$ a^{-1} from modelling gas production in small-scale laboratory experiments (Small et al., 2006) and $4.73 \cdot 10^{-4}$ a^{-1} from modelling a large-scale gas generation experiment (Small et al., 2017). The rate constant used for the decomposition of readily degrading LMW organic matter in this study ($2.10 \cdot 10^{-3}$ a^{-1}) is thus in good agreement with the available experimental data. Note, however, that the hydrolysis constant reported by Small and co-workers refers to gas generation under near-neutral pH conditions. This suggests that the constant used in this study may overestimate the degradation of LMW organics in strongly alkaline conditions, while it seems to be

suitable for modelling the degradation of organics under the conditions of a degraded cementitious matrix.

To the best of our knowledge, degradation rates for slowly degrading organic matter have not yet been reported. It is expected that the degradation of PVC is very unlikely to occur in anaerobic, strongly alkaline conditions and at limited water availability, while it has been noted that well supported experimental data are lacking (Warthmann et al., 2013). Small et al. (2006) estimated the rate constant of hydrolysis of less reactive, polymeric cellulose to be $1.35 \cdot 10^{-4}$ a^{-1}. These authors considered hydrolysis as the rate-determining step during cellulose degradation. The rate determined by Small et al. (2006) is less than a factor 4 higher as compared to the value used for the degradation of PVC in this study. The decomposition model for organic matter anticipates that readily degradable organic compounds, such as reactive cellulose and other LMW organic materials, decompose within a few thousand years in anaerobic, strongly alkaline conditions, while PVC (and other polymeric materials) persist over a much longer time, i.e. at least up to a few ten thousand years.

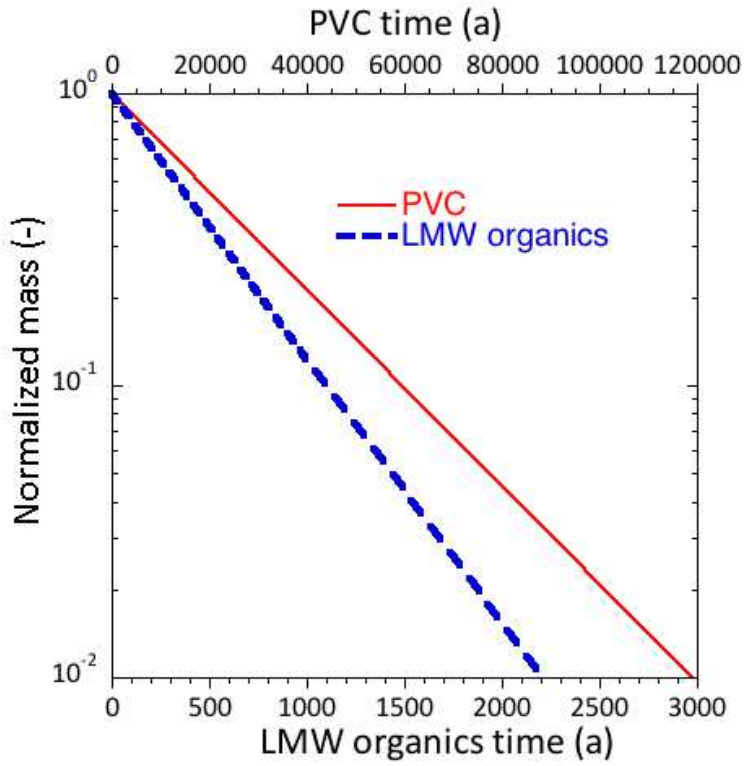

Figure 1: Kinetics of the degradation of LMW organics and PVC.

3.2 Carbonation of cementitious materials

Carbon dioxide (CO_2) produced during the decomposition of organic matter dissolves in the alkaline porewater, deprotonates to form its bases (HCO_3^{2-}, CO_3^{2-}) and, upon supersaturation, precipitates as calcium carbonate. The latter reaction gives rise to the conversion of Ca-bearing cement phases, in particular portlandite ($Ca(OH)_2$) and C-S-H phases ($xCaO \cdot SiO_2 \cdot nH_2O$) into calcium carbonate. Reaction of CO_2 with the main Ca-bearing phases can be expressed as follows:

$$Ca(OH)_2(s) + CO_2\,(aq) \Leftrightarrow CaCO_3(s) + H_2O \quad (2)$$

$$(CaO)_{1.667} \cdot SiO_2 \cdot (H_2O)_{2.1}(s) + 1.667\ CO_2(aq) \Leftrightarrow 1.667\ CaCO_3(s) + SiO_2(s) + 2.1\ H_2O \quad (3)$$

$$(CaO)_{0.833} \cdot SiO_2 \cdot (H_2O)_{1.33}(s) + 0.833\ CO_2(aq) \Leftrightarrow 0.833\ CaCO_3(s) + SiO_2(s) + 1.33\ H_2O \quad (4)$$

The stoichiometry shows that water is released during carbonation in addition to SiO_2 and it plays an important role in the kinetics of carbonation processes. Carbonation requires water, which acts as a catalyst, even though the reactions releases water from a stoichiometric perspective. Carbonation was found to be most efficient at a humidity of 50-70% (Lagerblad, 2005).

3.3 Corrosion of metals

A cement-stabilised waste form likely contains a small volume of air due to voids and air-filled porosity present in the waste package, while no information on the exact volume of air is available. Hence, oxic corrosion of metals is likely to occur in the early stage of the evolution of the waste form. This stage will be short as the inventory of oxygen is limited and residual oxygen will be consumed shortly after sealing the waste package. Thus oxic corrosion of metals is negligible and the corrosion of metals will be anoxic in humid/wet conditions in the long term, which produces hydrogen gas ($H_2(g)$) according to the following reactions:

Aluminium: $Al(s) + 3\ H_2O(l) \rightarrow Al(OH)_3(s) + 3/2\ H_2(g)$

Brass: $CuZn(s) + 4\ H_2O(l) \rightarrow Zn(OH)_2(s) + Cu(OH)_2(s) + 2\ H_2(g)$

Iron/steel: $3\ Fe(s) + 4\ H_2O(l) \rightarrow Fe_3O_4(s) + 4\ H_2(g)$

Zinc: $Zn(s) + 2\ H_2O(l) \rightarrow Zn(OH)_2(s) + H_2(g)$

Time-dependent metal corrosion can be represented by a zero-order kinetics:

$$m_{Fe}(t) = m_{Fe}(0) - kt \quad \text{(mol)} \tag{5a}$$

k: pH-dependent and surface area-adapted constant (mol a^{-1})

$m_{Fe(0)}$: Initial inventory of metal (mol)

with $k = \frac{R \cdot A \cdot \rho}{M}$ (5b)

R: Steady-state corrosion rate of metal (m a^{-1}) (Table 4)

A: Surface area of metal in the waste form (m^2) (Table 4)

ρ: Density of metal (Fe = 7855 kg m^{-3}; Al = 2710 kg m^{-3}, Zn = 7130 kg m^{-3}, brass = 8400 kg m^{-3})

M: Molar mass of metal (Fe = 0.05585 kg mol^{-1}, Al = 0.02698 kg mol^{-1}, Zn = 0.06539 kg mol^{-1}, brass: 0.06447 kg mol^{-1} (1:1 Cu:Zn stoichiometry)

The steady-state corrosion rates correspond to reference values currently used for modelling the gas generation in deep geological repositories (Diomidis, 2014; Diomidis et al., 2016; Poller et al., 2016). MIRAM 14 databases also include a compilation of the surface areas of the various metallic wastes (Nagra, 2014). This information was used to calculate the effective corrosion rates of metals in the waste form (Table 4). The modelling approach does not account for changes in the specific surface areas of the materials with time on the basis of specific geometric models, thus implying that surface areas are constant in the course of the temporal evolution of the waste form.

Table 4: Corrosion rates, surface areas and kinetic constants used for simulating the corrosion of aluminium, brass, iron/steel and zinc.

	R[a] (m a^{-1})	Surface area[b] (m^2)	k[c] (mol s^{-1})
Aluminium	$1.0 \cdot 10^{-5}$	2.350	$7.48 \cdot 10^{-8}$
Brass	$1.0 \cdot 10^{-4}$	29.60	$1.22 \cdot 10^{-5}$
Iron/steel alkaline conditions (pH ≥ 10.5)	$2.0 \cdot 10^{-8}$	413.78	$3.68 \cdot 10^{-8}$
Iron/steel near-neutral conditions (pH < 10.5)	$2.0 \cdot 10^{-6}$	413.78	$3.68 \cdot 10^{-6}$
Zinc	$1.0 \cdot 10^{-4}$	3.12	$1.08 \cdot 10^{-6}$

[a] Table 4.4 in Diomidis (2014);

[b] Surface areas as given in Nagra (2014);

[c] Estimated from Eq.(5b).

3.4 Internal degradation of cementitious material

The modelling scenario implies that the solidifying cementitious material will be fabricated either by using siliceous aggregate (e.g. quartz sand, sand etc.) or calcareous aggregate (e.g. limestone), respectively (Table 2). The presence of significant amounts of alkali hydroxides in the HTS cement gives rise to a high pH of the pore solution, which promotes the dissolution of siliceous aggregates in a cementitious environment. Silica release from siliceous aggregates is a commonly observed process in ageing cementitious material structures (e.g. Bérubé et al., 2000). In contrast, calcite is very stable in cementitious environments and therefore, the use of calcareous aggregate does not promote internal degradation of cementitious material.

The dissolution kinetics of quartz, used as a surrogate for siliceous aggregate (sand), can be expressed in terms of a (simplified) pH-dependent rate as reported by Palandri and Kharaka (2004) for neutral and alkaline conditions:

$$R_{dis}(t) = \frac{dm}{dt} = A\left(k_1\left(1-\Omega\right) + k_2 a_{H^+}^{-0.5}\left(1-\Omega\right)\right) \quad (\text{mol s}^{-1}) \qquad (6)$$

A: Reactive surface area (m^2)

k: Rate constants in neutral (k_1) and alkaline (k_2) conditions (mol s^{-1} m^{-2})

log k_1 = -13.99; log k_2 = -16.29

a_{H^+}: Activity of protons

Ω: Saturation index

The dissolution rate depends on the saturation index, Ω, which gradually changes from 0 to 1 while approaching equilibrium.

In this study the mass of siliceous aggregate (quartz) is considered to decrease by zero-order kinetics:

$$m_{SiO_2}(t) = m_{SiO_2}(0) - A(t)^* \cdot k^* \cdot t \quad (\text{mol}) \qquad (7)$$

$m_{SiO_2}(0)$: Initial inventory of siliceous aggregate (mol)

A(t)*: Time-dependent reactive surface area (m^2) ($A(t)^* = m_{SiO_2}(t) \cdot A(t)$) with A(t) as the molar area of the solid (m^2/mol)

k*: $k^* = k_1\left(1-\Omega\right) + k_2 a_{H^+}^{-0.5}\left(1-\Omega\right)$ (mol s^{-1} m^{-2})

Changes in the surface area and pH modify the dissolution rate. The specific surface area (A_s in m^2/g) is expected to increase with time as the size of particles decreases with time. In contrast, a decrease of the reactive surface area has been proposed elsewhere (Cochepin et al., 2008). However, it is currently uncertain as to what extent the reactive surface area actually changes in the course of the dissolution of siliceous aggregate. While the specific surface area increases with time, the reactive surface area per moles of particles may not significantly change with time due to precipitation of secondary phases on the surface of aggregates. In view of the latter uncertainty, the reactive surface area per moles of particles was assumed to be constant, i.e. A(t) = A(0) = constant in Eq. (7). Grain size and inventory of the aggregate used to fabricate the solidifying cementitious material are listed in Table 5.

Table 5: Aggregate: Inventory, grain size, and initial surface area.

Inventory of aggregate[a] (kg)	Grain size diameter[b] (mm)	Initial surface area[c] A(0) (m^2)	Initial GEMS surface area[d] A(0) (m^2 mol^{-1})
1971.58	*1.5*	2976.00	$9.07 \cdot 10^{-2}$

[a] See Table 7. The inventory of aggregate corresponds to that of aggregate added (Table 1) plus the LOI of cement (Table 3);
[b] Estimated grain size;
[c] Estimated for the inventory of aggregates by assuming spheres at the given grain size;
[d] Reactive surface area (A(0)) as implemented in GEMS.

4. Modelling approach

4.1 Geochemical modelling set-up

The geochemical modelling set-up corresponds to that reported elsewhere (Wieland et al., 2018):

1) The GEM-Selektor (GEMS) v3.3 code was used (Kulik et al., 2013);

2) The basic thermodynamic properties of the aqueous species, the minerals and cement phases were assigned according to the Nagra/PSI thermodynamic database (Hummel et al., 2002; Thoenen et al., 2014) and the CEMDATA 14.01 database (Lothenbach et al., 2012b);

3) Uptake of alkalis by C-S-H phases was modelled using an ideal solid solution model between jennite, tobermorite, $[(KOH)_{2.5}SiO_2H_2O]_{0.2}$ and $[(NaOH)_{2.5}SiO_2H_2O]_{0.2}$, and the thermodynamic properties listed in Wieland et al. (2018) that had previously been derived by Kulik et al. (2007) and Lothenbach et al. (2012a);

4) Thermodynamic properties of zeolites were selected from the Thermoddem database (Blanc et al., 2012);

5) Thermodynamic data of Zn and Cu species were selected from the SUPCRT92 database (Helgeson et al., 1978; Johnson et al., 1992);

6) Thermodynamic data of chloride salts were selected from the SUPCRT92 database (halite, sylvite) and according to Robie and Hemingway (1995) (chloromagnesite, hydrophilite and laurencite);

7) Modelling was performed at standard conditions (T = 25°C and 1 bar);

8) Ionic strength corrections in GEMS were calculated based on the built-in extended Debye-Hückel equation applicable up to about I = 1 M (parameters: a_i = 3.31 Å, b_y = 0.098 for NaOH electrolyte at 25 °C).

Thermodynamic properties of the relevant species are listed elsewhere (Kosakowski and Berner, 2013). Minerals and cement phases found to be relevant for this study are listed in Table 6. The inventories of some minerals were found to be very low compared to the main minerals and cement phases, such as pyrite, zincite, sphalerite, cuprite and chalcocite. Nevertheless, they are displayed in the plots, although hardly visible, in order to account for the products formed in the presence of brass, copper and zinc. In addition to the minerals listed in Table 6, the formation of other minerals was observed, such as celestite, strontianite, barite and witherite. These minerals are not displayed, as their amounts are small due to the low Sr and Ba contents of cement.

4.2 Cement paste

Thermodynamic modelling of the hydration process was carried out to quantify the mineral composition and important solution parameters of the solidifying cementitious material at equilibrium. Kinetics of the hydration process was not taken into account as it is plausible to assume that the hydration process is completed within a short period of time compared to the period of concern for the L/ILW repository (10^5 years). Furthermore, it was assumed that both silica fume and clinoptilolite are supplementary materials with the same reactivity, and therefore, completely dissolve in the course of the hydration process. The input parameters used for modelling cement hydration are listed in Table 2 (siliceous aggregate in normal type, calcareous aggregate in italic type) and Table 3. The results are discussed below.

4.3 Simplifications

1) Copper was treated in terms of equilibrium chemistry (instantaneous reaction), while the dissolution of aluminium, brass, iron/steel and zinc was controlled by kinetics.

2) Thermodynamic data of both magnetite (Fe_3O_4) and hydromagnetite ($Fe_3O_4 \cdot 2H_2O$) were included in the thermodynamic database, thus taking into account also the higher solubility of hydromagnetite (Kosakowski and Berner, 2013). Note, however, that the total mass of magnetite and hydromagnetite is displayed.

3) The total mass of Mg-bearing carbonates (dolomite and magnesite) is shown.

4) The formation of zeolites was either allowed or suppressed with the aim of assessing the effect of zeolite formation on the chemical evolution of the waste form. The inventory of zeolites is given in terms of the total amount of all zeolite-type minerals that were formed. Zeolite formation in cementitious systems was considered previously by Kosakowski and Berner (2013), and the subject is further discussed in Lothenbach et al. (2017).

Table 6: Important minerals and cement phases of the mineral assemblage. The thermodynamic properties are listed in Kosakowski and Berner (2013).

Mineral	Composition	Mineral	Composition
Calcite	$CaCO_3$(cr)	Gibbsite	$Al(OH)_3$(s)
C-S-H	see text	Kaolinite	$Al_2Si_2O_5(OH)_4$(s)
Portlandite	$Ca(OH)_2$(cr)	Quartz	SiO_2(cr)
(Al/Fe)-Si Hydro-garnet ss	$Ca_3(Al/Fe)_2(SiO_2)O_6{\cdot}4H_2O$	am. Silica	SiO_2(s)
Ettringite	$Ca_6Al_2(SO_4)_3(OH)_{12}{\cdot}26H_2O$	Zeolites	
Strätlingite	$Ca_2Al_2(SiO_2)(OH)_{10}{\cdot}3H_2O$	- Analcime	$NaAl(Si_2O_6){\cdot}H_2O$
AFm phases e.g.		- Clinoptilolite	$Ca_3(Al_6Si_{30})O_{72}{\cdot}20H_2O$
- Monocarbonate	$Ca_4Al_2(CO_3)O_6{\cdot}11H_2O$	- Chabazite	$(Ca_{0.5},Na,K)_4[Al_4Si_8O_{24}]{\cdot}12H_2O$
- Friedel's salt	$Ca_4Al_2Cl_2(OH)_{12}{\cdot}4H_2O$	- Scolecite	$CaAl_2Si_3O_{10}{\cdot}3H_2O$
- Kuzel's salt	$Ca_4Al_2Cl(SO_4)_{0.5}(OH)_{12}{\cdot}6H_2O$	- Laumontite	$Ca(AlSi_2O_6)_2{\cdot}4H_2O$
Hydrotalcite	$Mg_4Al_2(OH)_{14}{\cdot}3H_2O$	- Ca-Phillipsite	$Ca_3Al_6Si_{10}O_{32}{\cdot}12H_2O$
Magnetite	Fe_3O_4	- K-Phillipsite	$K_6Al_6Si_{10}O_{32}{\cdot}12H_2O$
Hydromagnetite	$Fe_3O_4{\cdot}2H_2O$(s)	- Na-Phillipsite	$Na_6Al_6Si_{10}O_{32}{\cdot}12H_2O$
Pyrite	FeS_2(cr)		
Siderite	$FeCO_3$(cr)	Chloride salts	
Dolomite	$CaMg(CO_3)_2$(cr)	- Halite	NaCl(cr)
Magnesite	$MgCO_3$(cr)	- Sylvite	KCl(cr)
Zincite	ZnO(cr)	- Chloromagn.	$MgCl_2$(cr)
Sphalerite	ZnS(cr)	- Hydrophilite	$CaCl_2$(cr)
Cuprite	Cu_2O(cr)	- Laurencite	$FeCl_2$(cr)
Chalcocite	Cu_2S(cr)		

4.4 Modelling strategy

The modelling approach corresponds to that reported earlier by Wieland et al. (2018). It is based on the following step-by-step procedure:

i) The inventory of waste materials was selected from the MIRAM database and arranged for the geochemical modelling, e.g. by combining urea and LMW organics;

ii) The initial composition of the solidifying cementitious material used for conditioning the waste was modelled;

iii) The effect of the degradation of organic waste materials, metal corrosion and internal degradation of cementitious material in the presence of siliceous aggregate on the

temporal evolution of the chemical condition in the waste package was modelled. Note that the latter process is not relevant in the case of calcareous aggregate.

Three modelling scenarios were considered: 1) use of either siliceous or calcareous aggregate; 2) formation or absence, respectively, of zeolites; 3) limited and unlimited water availability.

5. Results

5.1 Initial conditions

The phase assemblage and solution composition of the solidifying cementitious material corresponds to a "low pH" cement (Table 7). According to the thermodynamic calculations, portlandite was completely converted into C-S-H phases (calcium silicate hydrate with variable composition) by the addition of large amounts of silica fume and clinoptilolite (Table 2). Note that portlandite was formed in the first stage of the hydration process, while it was consumed by pozzolanic reaction with siliceous materials in the subsequent stage. The initial pH was 12.68 and the Ca/Si ratio of the C-S-H phases was relatively low (Ca/Si ratio = 1.01). Ettringite (AFt, Al_2O_3-Fe_2O_3-tri phase), Al/Fe siliceous hydrogarnet (Fe(III)-bearing phase), hydrotalcite (Mg-bearing phase), and calcite were the main constituents of the cement paste in addition to C-S-H phases (Table 7). Interestingly, the formation of AFm phases (Al_2O_3-Fe_2O_3-mono phases) was not observed likely due to the relatively large SO_3/Al_2O_3 ratio of the cement. The E_h value was positive (0.45 V), indicating initially oxidising conditions (Table 7). Replacing siliceous by calcareous aggregate had, besides differences in the quartz and calcite inventories, no significant effect on the composition of the hydrate assemblage, as well as on the composition of the pore solution at equilibrium. It should be noted that modelling the composition of the solidifying cementitious material implicitly assumes that the time required to reach the equilibrium state of the cement paste is much shorter than the period of concern for the L/ILW repository.

Table 7: Initial conditions of the cementitious matrix with either siliceous (quartz) or calcareous aggregate (limestone). Thermodynamic calculations were performed using the input data listed in Tables 2 and 3.

Cementitious material mix	Quartz	Limestone
- w/c ratio[a]	0.61	0.61
- w/b ratio[a]	0.47	0.47
- cement/aggregate ratio	0.64	0.64
- bulk density (g cm^{-3})	2.33	2.35
- dry density (g cm^{-3})	2.50	2.52
- total volume (dm^3)	1941.16	1924.40
- total mass (aq. + sol.) (kg)	4518.97	4519.00
- pH	12.68	12.68
- E_h (V)[b]	0.45	0.45
- Ionic strength (mol kg^{-1})	0.172	0.172
Solids and aqueous phase	Quartz	Limestone
	Mass (kg)	
- Portlandite	0	0
- C-S-H	1891.53	1891.53
- Ca/Si ratio	1.01	1.01
- Ettringite	140.10	140.10
- Al/Fe-Si hydrogarnet	220.50	220.50
- Hydrotalcite	29.22	29.22
- Calcite	45.47	1995.47
- Barite	$3.8 \cdot 10^{-2}$	$3.8 \cdot 10^{-2}$
Quartz[c]	1971.58	21.60
Aqueous phase	220.55	220.55

[a] w/c ratio: water-to-cement ratio, w/b ratio: water-to-binder ratio (= cement plus silica fume plus clinoptilolite);

[b] E_h: Electrode potential relative to standard hydrogen electrode (SHE);

[c] Quartz accounts for the total inventory of quartz sand and sand as listed in Table 1. The difference between input data for inert quartz (Table 1) and the output can be attributed to the loss on ignition (LOI) of HTS cement (Table 3) which was assumed to be an "inert phase" with the properties of quartz (Berner, 2009).

5.2 Chemical evolution at limited water availability

Geochemical modelling of the waste form was performed on the assumption that only free water entrapped in the waste package was available for reaction (Figures 2 and 3). This assumption implies that the containment of the waste form remains "intact" and that water cannot enter the

waste package. Hence, the amount of water in the waste package corresponds to water entrapped in the pore space of the solidifying cementitious material. As the amount of free water was limited, the reactivity of this waste form ceased already at ~ 1500 years, if siliceous aggregate was used for fabrication of the solidifying cementitious material and zeolites were formed (Figure 2). At this point in time, the reactivity of the waste form came to a halt according to the thermodynamic calculations and the pH remained stable. Metal corrosion was the dominant water-consuming reaction, as the inventories of organic materials (LMW, PVC) were low compared to the total material inventory. Thus, iron/steel corrosion consumed water and limited the reactivity of this waste form (Figure 2).

The absence of portlandite lowered the pH at which the buffering capacity of the cement paste was active, which had an effect on the pH evolution (Figure 2d). According to the current modelling assumption, portlandite was not formed during cement hydration (Table 7) due to the large amount of silica fume and clinoptilolite added (Table 2). Quartz sand with a relatively low particle size was used as siliceous aggregate, which is the main Si source of the waste form (Tables 2 and 5). Siliceous aggregates dissolve in the highly alkaline cement pore water with time, which allowed for a continuous conversion of C-S-H phases with an intermediate Ca/Si ratio (1.01) into C-S-H phases with a low Ca/Si ratio (0.79) (Figure 6). Zeolites were thermodynamically stable at ~ 200 years (Figure 2b) as a result of a pH drop below 12.5 and due to the presence of a Si source. The pH steadily dropped from initially 12.68 to ~ 10.5 as a result of alkali uptake by zeolites and the low Ca/Si C-S-H phases, which is reflected by a continuous decrease of the aqueous alkali concentration (Figures 2d/e). Iron/steel corrosion was accelerated below pH 10.5. The influence of zeolites on the pH evolution was observed when modelling the same system on the assumption that zeolite formation was inhibited (data not shown). In this case, pH > 10.5 was maintained over the entire period of reactivity of the waste form.

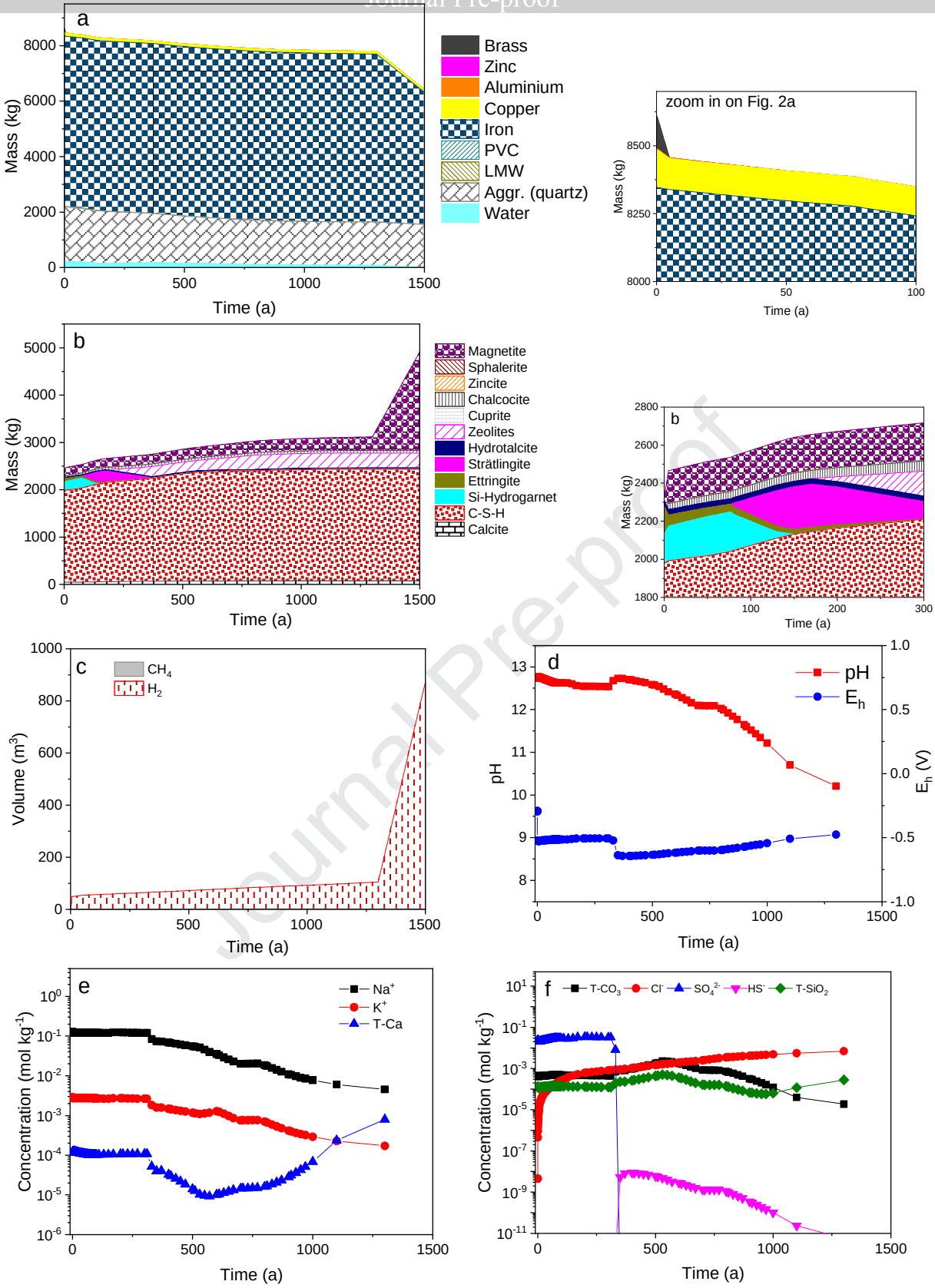

Figure 2: Time-dependent evolution of the waste form at limited water content, siliceous aggregate, and possible formation of zeolites, a) waste materials and aggregate (left) and zoom in (right), b) cement phases and minerals (left) and zoom in (right), c) gas production, d) pH and E_h, e) major cations (T-Ca = total Ca), f) major anions ($T\text{-}CO_3$ = total carbonate; $T\text{-}SiO_2$ = total silica).

Temporal evolution of the mineral composition of cement paste revealed thermodynamic instability of all cement phases, except C-S-H phases, before ~ 400 years (Figure 2b). At the early stage, the main cement phases were ettringite (AFt), Al/Fe siliceous hydrogarnet, hydrotalcite and C-S-H phases, while strätlingite was formed as an intermediate phase.

Hydrogen was the main gaseous compound, while only traces of CH_4 were produced because of the low inventory of organic materials (Figure 2c, Table 1). As a consequence, also the amount of CO_2 produced with time was low and therefore, carbonation of C-S-H phases was limited. Hydrogen gas production drastically accelerated at ~ 1300 years, once the pH dropped below 10.5 due to the factor 100 higher corrosion rate of iron/steel at these conditions (Figures 2c/d).

The redox potential dropped from +0.45 V to values ranging between -0.51 V and -0.65 V as a result of O_2 consumption by oxic corrosion already in the early stage of the evolution of the waste form (Figure 2d). Reducing conditions stabilised the S(-II) redox state at the expense of S(VI) and therefore, HS^- was the main aqueous sulphur species (Figure 2f). The reduction of S(VI) to sulphur species with lower oxidations states was observed in Fe(0)-containing slag cements, suggesting that the reduction may not be kinetically hindered in iron/steel-containing waste forms (e.g. Lothenbach and Gruskovnjak, 2007; Gruskovnjak et al., 2011). As a consequence, ettringite, which is the main SO_4^{2-} source in cement paste, was destabilised with time. The aqueous Cl^- concentration continuously increased as a result of PVC degradation in all scenarios. Nevertheless, the maximum Cl^- concentration was below 0.1 M due to the low inventory of PVC (Figure 2f). Na^+ was the main charge-compensating cation in all conditions (Figure 2e).

Temporal evolution of the chemical conditions of the waste form with calcareous aggregate revealed notable differences compared to the waste form containing siliceous aggregate (compare Figures 2 and 3). Reactivity of the waste form was extended to ~ 8500 years due to limited water availability and zeolites were not formed in the presence of calcareous aggregate (Figure 3b). The absence of a substantial Si source (i.e. siliceous aggregate) and the high pH prevented zeolite

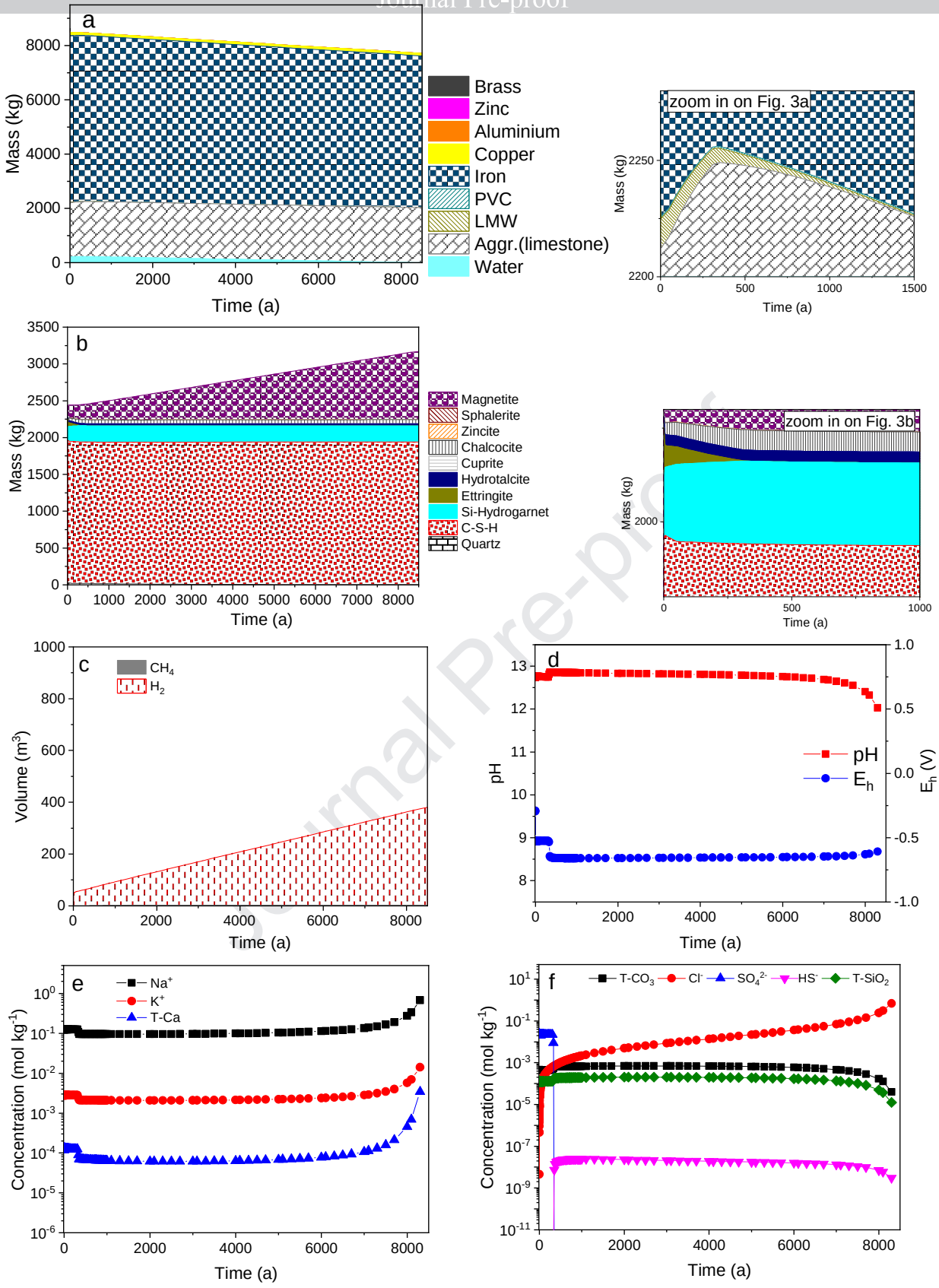

Figure 3: Time-dependent evolution of the waste form at limited water content, calcareous aggregate, and possible formation of zeolites, a) waste materials and aggregate (left) and zoom in (right), b) cement phases and minerals (left) and zoom in (right), c) gas production, d) pH and E_h, e) major cations (T-Ca = total Ca), f) major anions (T-CO_3 = total carbonate; T-SiO_2 = total silica).

formation (Figure 3d). As a consequence of this, the pH was stabilised above 10.5, and H_2 was continuously produced in accordance with the slow corrosion of iron/steel at pH ≥ 10.5. The apparent decrease of pH after ~ 8000 years is a consequence of significant reduction of the small amount of free water available in the waste package, which resulted in a strong increase in the Cl^- concentration.

The use of calcareous instead of siliceous aggregate had an effect on the evolution of the mineral assemblage, besides the absence of zeolites (Figure 3b). Magnetite was steadily formed with time due to slow corrosion of iron/steel in the highly alkaline cement porewater and Al/Fe siliceous hydrogarnet was thermodynamically stable over the entire period of time to the end of reactivity of the waste form. C-S-H was the dominant cement phase. The Ca/Si ratio of C-S-H changed only slightly from initially 1.01 to 0.96 after ~ 8500 years as a result of the small amount of quartz that was present in the waste form (associated with LOI). The pH was stabilised above 12.5 as the major sinks for the alkalis, i.e. zeolites and C-S-H phases with a low Ca/Si ratio, were absent. The aqueous alkali concentration was high over the entire period of reactivity of the waste form.

The modelling results may be of limited accuracy at the very end of the reactivity of the waste form for both scenarios, i.e. with siliceous and calcareous aggregates, due to the very limited amount of water available in this stage. For example, the aqueous concentrations of all solutes may be strongly increased which results in ionic strengths > 1 mol/kg, the threshold molality allowed for activity corrections with the applied Debye-Hückel approach. Furthermore, the strong increase in the Cl^- concentration may affect the corrosion rate of steel and iron, while little is known about the degradation kinetics and dissolution of silicates in brine-like conditions. Hence, the model predictions available for the last few time steps before the reactivity of the waste form comes to a halt, i.e. beyond 1400 years in the scenario with siliceous aggregate and beyond 8000 years in the scenario with calcareous aggregate, are associated with large uncertainties.

5.3 Chemical evolution at unlimited water availability

Geochemical modelling of the waste form at unlimited water availability accounts for the temporal evolution of the chemical conditions over the entire period of concern for the L/ILW repository. Unlimited water availability implies that the containment of this waste form does not remain “intact”, and gas can escape (and enter) through one or more small openings or by vents, such as small holes drilled in the walls of the drums (mm diameter or smaller). In this case, availability of water is not limited by free water in the waste package, but by the humidity outside the containment and vapour transport from the surrounding backfill into the waste package.

As previously mentioned, the corrosion of iron/steel was completed within less than a few thousand years once pH dropped below 10.5 in the system with siliceous aggregate (Figure 4). With calcareous aggregate, however, iron/steel corrosion proceeded at the very low rate assigned to highly alkaline conditions (i.e. pH ~ 12.7) (Figure 5c). The gas phase was mainly composed of H_2 in the long term, as the inventory of organics, producing CO_2 and CH_4 during decomposition of organic matter, was low.

Temporal evolution of the mineral composition revealed that all cement phases, with the exception of C-S-H phases, were chemically unstable already in the very early stage of the evolution of this waste form, i.e. before ~ 400 years. C-S-H phases, however, were present over the entire period of concern for the L/ILW repository, also in the waste form containing siliceous aggregate (Figure 4b). In the long term, in the modelling scenario with siliceous aggregate, the main constituents of the mineral assemblage were C-S-H phases, quartz and magnetite in addition to small amounts of calcite and zeolites. In the modelling scenario with calcareous aggregate, the main constituents were C-S-H phases, calcite and magnetite in addition to small amounts of Al/Fe siliceous hydrogarnet and quartz. Hydrotalcite, gibbsite, zincite, sphalerite, cuprite and chalcocite were found to be minor constituents of the mineral assemblage in all modelling scenarios.

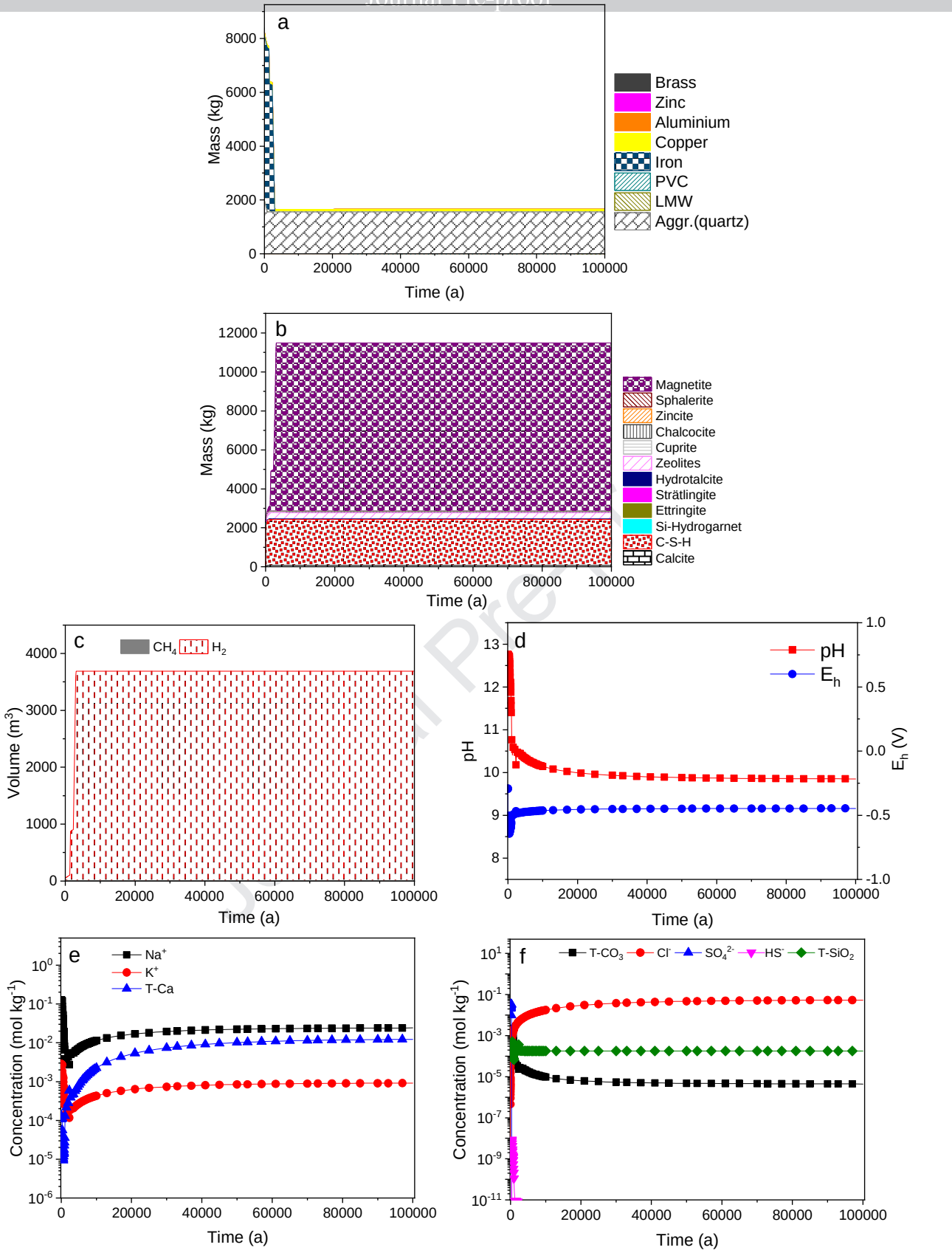

Figure 4: Time-dependent evolution of the waste form at unlimited water content, siliceous aggregate, and possible formation of zeolites, a) waste materials and aggregate, b) cement phases and minerals, c) gas production, d) pH and E_h, e) major cations (T-Ca = total Ca), f) major anions (T-CO_3 = total carbonate; T-SiO_2 = total silica).

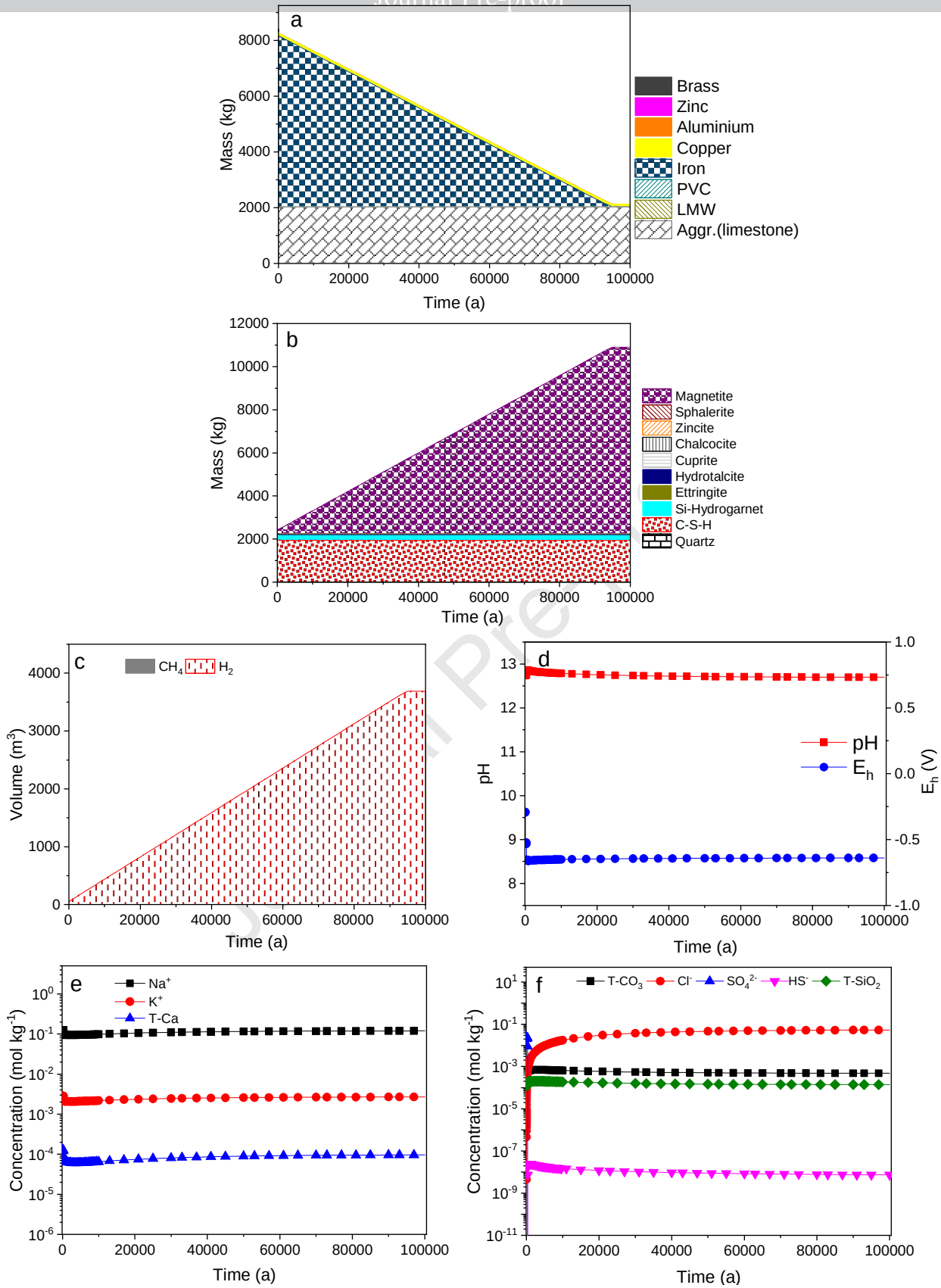

Figure 5: Time-dependent evolution of the waste form at unlimited water content, calcareous aggregate, and possible formation of zeolites, a) waste materials and aggregate, b) cement phases and minerals, c) gas production, d) pH and E_h, e) major cations (T-Ca = total Ca), f) major anions (T-CO_3 = total carbonate; T-SiO_2 = total silica).

In the long term, the porewater chemistry was dominated by Cl^- as anion and Na^+ as the charge-compensating cation in solution for both systems, i.e. with either siliceous or calcareous aggregate, respectively (Figures 4e/f and 5e/f). Note that Cl^- was steadily released to solution by the degradation of PVC. The pH dropped to either ~ 9.9 in the system with siliceous aggregate, while the pH was buffered at ~ 12.7 in the waste form with calcareous aggregate (Figures 4d and 5d). In the latter case, Na^+ uptake by C-S-H phases and zeolites was limited and OH^- was an important aqueous anionic species in addition to Cl^-. In both systems, the E_h ranged between -0.45 V and -0.64 V in the long term (Figures 4d and 5d). Reducing conditions stabilised the S(-II) redox state at the expense of S(VI). Thus, HS^- was the dominant aqueous sulphur species, and its concentration was controlled by the solubility of sphalerite and chalcocite.

6. Discussion

The relevant processes of waste degradation include the corrosion of metals (aluminium, brass, iron, steel, zinc), the decomposition of organic materials and subsequent carbonation of cementitious material as well as the dissolution of siliceous aggregate (quartz). These processes, and, in particular, the interaction of the reaction products (e.g. CO_2) with the cement matrix, determine the long-term evolution of the chemical conditions of the waste form.

Geochemical modelling enables us to assess the long-term behaviour of the specific waste form considered in this study in view of the following initial conditions:

Absence of portlandite: The initial hydrate assemblage of cement pastes is composed of main cement phases, in particular C-S-H phases, ettringite, Al/Fe siliceous hydrogarnet, hydrotalcite and calcite while portlandite is absent. Significant amounts of silica fume (“Micropoz”; 375 kg) and less clinoptilolite (187 kg) are added during fabrication of the solidifying cementitious material and, as a consequence, portlandite is completely converted into C-S-H phases during cement hydration. Thus, the composition of the hydrate assemblage corresponds to that of a cement paste reported

for so-called "low pH" cements (e.g. Cau Dit Coumes et al., 2006; Garcia Calvo et al., 2010; Lothenbach et al., 2014; Rossen et al., 2015). The absence of portlandite significantly reduces the pH at which the pH buffering capacity of the cement paste is active. The Ca/Si ratio of C-S-H phases is lower than in a portlandite-containing cement paste, which lowers the initial equilibrium pH to 12.68 (Table 7). Thus, the cement paste of the solidifying cementitious matrix has already reached an altered stage in the degradation process of cements compared to a cement paste prepared in the absence of large amounts of supplementary cementitious materials. It has to be noted that the same reactivity has been assigned to silica fume (micron-sized) and clinoptilolite (sand grade) in this study, which is a conservative assumption as it may overestimate the reactivity of clinoptilolite and therefore, the availability of silica in the pozzolanic reaction. Further assessment of the current modelling approach will also require an alternative scenario to be considered where clinoptilolite has the same reactivity as siliceous aggregates with comparable grain size rather than the reactivity of a supplementary cementitious material.

Water availability: The availability of water determines the period of time over which the waste form is reactive because all degradation reactions (metal corrosion, decomposition of organics, dissolution of siliceous aggregate) consume water, while carbonation is the only reaction releasing water. The pore water of cementitious material is likely to provide a connected water phase, which allows diffusion of water and solutes in the waste package. With time, however, water is consumed by the aforementioned reactions and gas is produced. After some time, water flow/diffusion could be inhibited as pores are filled with gas or, to some extent, carbonate as a result of carbonation, given that water is available to catalyse carbonation. Replacing siliceous by calcareous aggregate extends the period of reactivity of the waste form in the modelling scenario with limited water availability. The latter scenario implies that only water entrapped during waste conditioning in the pore space of the solidifying cementitious material is available for waste

degradation and dissolution of siliceous aggregate. The period of water availability is mainly determined by iron/steel corrosion, as water is rapidly consumed once accelerated iron/steel corrosion starts. Note that iron/steel corrosion is completed within a few hundred up to few thousand years once pH drops below 10.5. The period of water availability is prolonged in the presence of calcareous aggregate as conditions remain highly alkaline, thus preventing accelerated iron/steel corrosion.

Overall, the evolution of pH in the waste form is a key factor determining the progress of iron/steel corrosion and the mineral composition of the cementitious backfill. The evolution of pH is controlled by the following processes:

Carbonation: The production of CO_2 by the decomposition of organic matter and conversion of the Ca-containing cement phases into calcite by carbonation governs the evolution of the chemical conditions of those waste forms with large inventories of degrading organic waste (Wieland et al., 2018). The degradation of organics may take place by microbial activity while hydrolysis of the organics is the rate-determining step (Small et al., 2008). Microbially mediated decomposition of organic matter could occur as the amounts of substrates (carbon source) and oxidants (electron acceptors) that are present in the waste matrix are considered to be large (Leupin et al., 2016). In contrast, however, microbial activity could be limited because of the harsh living conditions in a cementitious environment at pH 12 and above, while microbiological niches with a lower pH value could exist due to local heterogeneities in the waste form. Thus, an overall assessment of whether the degradation of organics occurs predominantly by chemical or microbial processes is presently difficult on the basis of the available information. For this study, it was assumed that i) the decomposition of organic matter is complete, ii) CO_2 and CH_4 production does not depend on pH, and iii) the degradation processes of readily and slowly degrading organics can be represented by the simplified models outline in section 3.1. In a previous study, it was further observed that the

type of aggregate has only a minor effect on the temporal evolution of the chemical conditions in waste forms with a large inventory of organic matter (Wieland, 2019). The waste form considered in this study has a low inventory of organics and therefore, carbonation is not a determining factor in the course of the evolution of this waste form.

Zeolite formation: Zeolites play an important role in controlling the pH evolution in addition to continuous conversion of C-S-H phases. Alkalis are taken up into the structure of some zeolites (Table 6) and therefore, formation of zeolites results in a steady decrease of the aqueous alkali concentration. The favourable effect of calcareous aggregate on the pH evolution and the prevention of zeolite formation is highlighted for the waste form considered in this study. Zeolites start forming already after ~ 200 years in the modelling scenario with siliceous aggregate, while zeolites are not formed in the presence of calcareous aggregate. The latter observation shows that the use of calcareous aggregate may prevent zeolite formation.

C-S-H phases: Replacing siliceous by calcareous aggregate influences the chemical composition of the C-S-H phases with time. Siliceous aggregate is chemically not stable in the highly alkaline cement pore water and progressively dissolves. Silica released in the course of the dissolution of siliceous aggregate reacts with C-S-H phases, thus converting C-S-H phases with a high Ca/Si ratio into C-S-H phases with a low Ca/Si ratio (Figure 6). The formation of C-S-H phases with a low Ca/Si ratio furthers alkali uptake. Hong and Glasser (1999) showed that alkali binding into C-S-H phases improves with decreasing Ca/Si ratio. This observation is further supported by recent studies (Bach et al., 2013; L'Hôpital et al., 2016). As a result, the pH decreases in those systems where the alkalis are the main cations in solution and OH^- is the main charge-compensating anion.

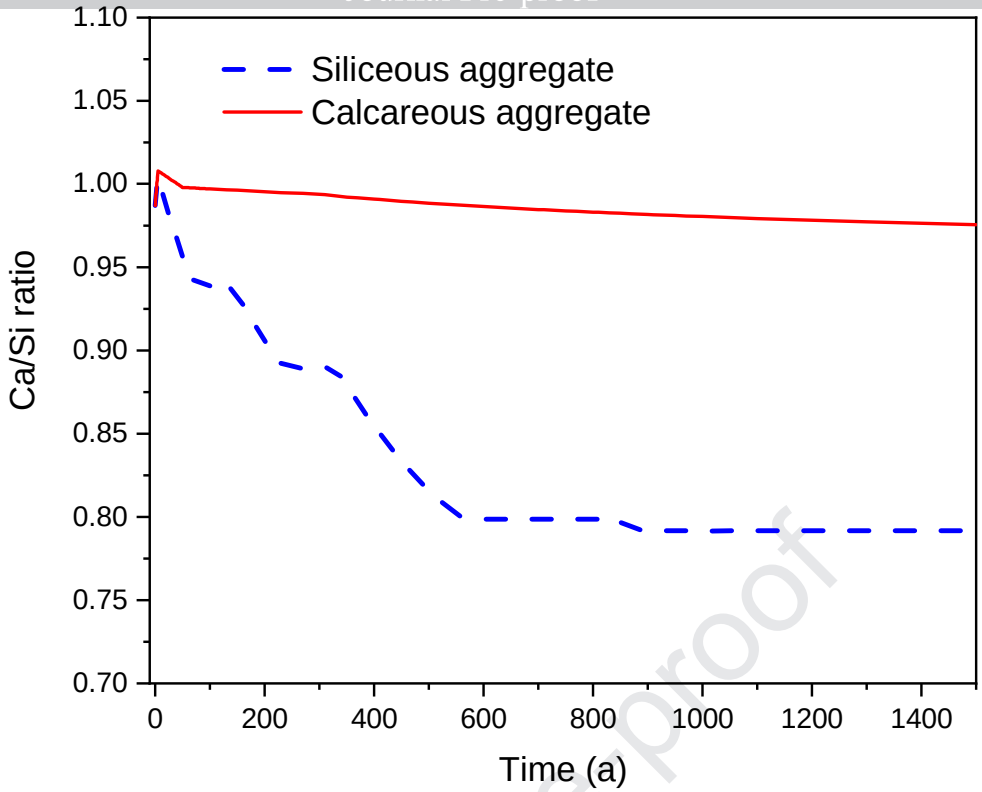

Figure 6: Time dependence of the Ca/Si ratio of C-S-H phases using siliceous or calcareous aggregates, respectively, for fabrication of the solidifying cementitious material.

The modelling further shows that C-S-H phases might persist in both systems, i.e. the waste forms produced with either siliceous or calcareous aggregates, respectively, over the entire period of concern for an L/ILW repository (10^5 years). C-S-H phases are the most important component of cementitious materials and, further, the most important sorbing material in the cement matrix for metal cations. Therefore, C-S-H phases play a decisive role in the retardation of cationic radionuclides due to their presence in the waste form over a very long period of time.

Presence of Cl^-: The degradation of PVC imposes an additional constraint on the evolution of the chemical conditions of this waste form. Cl^- is continuously released in the course of PVC degradation, which gives rise to continuous increase in the aqueous Cl^- concentration. The progressively increasing Cl^- concentration has an influence on the pH evolution over time. Cl^- becomes the main charge-compensating anion in solution instead of OH^-, which reduces the OH^- concentration in solution and thus the pH.

Modelling the long-term evolution of the waste form has been conducted on the assumption that water availability is not limited due to ingress of humidity through openings and vents. It should be noted that the transport of vapour could be influenced by gas produced in the waste package. The containment of the waste form thus plays a key role in the transport of water, solutes and gas between the different compartments, i.e. from the emplacement container and further into the backfill of the near field. The following findings are important in connection with the long-term evolution of the waste form:

Gas production: Corrosion of iron/steel is the main source of gas production (H_2) as the inventory of organics (giving rise to CH_4 production) is very low in this waste form. The temporal evolution clearly reflects the consequences of the assumptions made regarding the pH dependence of the corrosions rates, i.e. a factor 100 difference between the rates above and below pH 10.5. This assumption is based on our current knowledge about the dependence of corrosion rates on pH as reliable data are available at strongly alkaline conditions (typically pH > 12) and near-neutral conditions. To the best of our knowledge, however, no reliable data have been reported for the intermediate pH range. Nevertheless, a scenario for the temporal evolution of gas production can be anticipated by tentatively assuming a steady decrease in the corrosion rate with deceasing pH (linear interpolation between the two rates listed in Table 4). A linear increase in the corrosion rate with decreasing pH would result in larger gas volumes produced in the pH range between 12.68 (initial pH of waste form) and 10.5. For example, the H_2 production displayed in Figure 2c would be higher in the time period up to ~ 1300 years compared to present model. Nevertheless, once pH drops below pH 10.5 after ~ 1300 years, corrosion proceeds in accordance with a rate of 2 µm/a assigned to the pH range < 10.5 (Table 4). As a result, steel/iron corrosion is still completed within a few thousand years, as depicted in Figure 4c, which has been predicted based on the current model, i.e. two distinct rates assigned to pH above and below 10.5. Hence, the conclusions

drawn from the modelling are still sound at pH < 10.5, while they must be reconsidered regarding the temporal evolution of H_2 production in the pH range 10.5 to 12.68.

The current modelling approach specifically highlights the consequences on gas production by the type of aggregates used. Replacing siliceous by calcareous aggregates prevents the conversion of C-S-H phases with a high Ca/Si ratio into C-S-H phases with a low Ca/Si ratio, and also zeolite formation, as no additional silica source is available. Using siliceous aggregate results in a drop in pH below 10.5 and accelerated iron/steel corrosion coinciding with the production of a large H_2 volume within a short period of time compared to the period of concern for the L/ILW repository (Figure 7). Nevertheless, both processes are inhibited by using calcareous aggregate. Consequently, the pH is stabilised above the threshold value for accelerated iron/steel corrosion and therefore, the production of H_2 proceeds continuously at the very slow corrosion anticipated in strongly alkaline conditions over the period of concern for the L/ILW repository.

Waste volume: The degradation of organic waste produces gaseous CH_4 and CO_2. As a result of the formation of gaseous compounds, the volume of organic waste decreases with time. In contrast, iron/steel corrosion produces large volumes of H_2 and magnetite as corrosion product. For the model waste form considered in this study the reduction in the waste volume by the degradation of organic matter is negligible, while the formation of corrosion products increases the waste volume due to differences in the molar volume of iron and magnetite. The internal stress associated with the overall increase in volume may affect the mechanical stability of the waste form, in particular causing crack formation in the concrete casing. The overall volume changes may further have an effect on porosity of the waste form and consequently on water transport inside the container. It was noted that the extent of changes in the volume of a waste form depends on the iron/steel inventory and the ratio between the inventories of organic matter and iron/steel (Wieland et al., 2018).

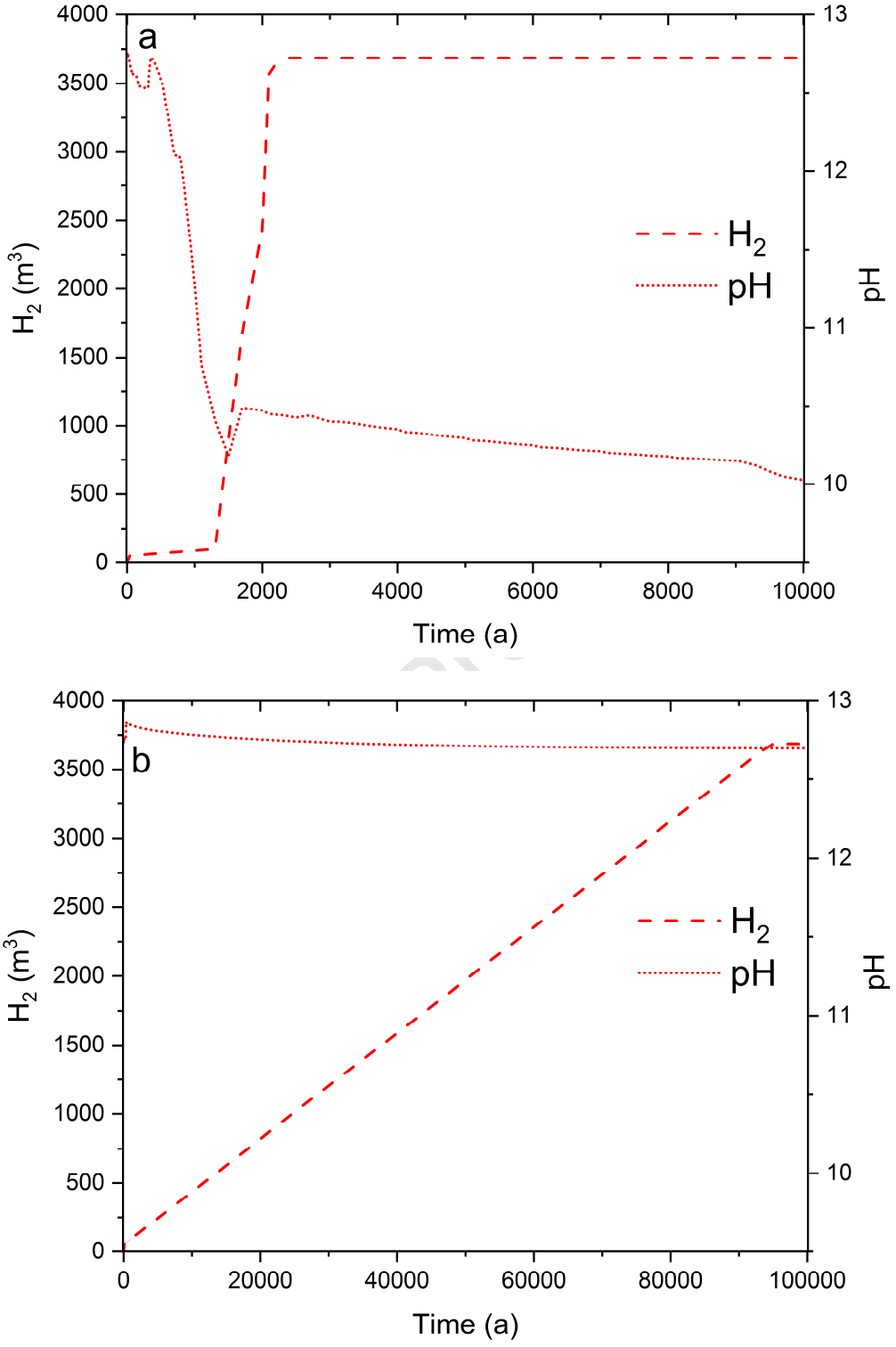

Figure 7: Temporal evolution of gas phase and pH in presence of a) siliceous aggregates and b) calcareous aggregates. Note that different scales of the x-axes are applied to the systems with siliceous and calcareous aggregates.

7. Conclusions

The chemical processes responsible for the degradation of waste materials and the solidifying cementitious material are i) corrosion of metals (aluminium, brass, iron, steel, zinc), ii) decomposition of organic compounds (LMW and polymeric materials), iii) carbonation of cementitious materials and corrosion products, and iv) internal degradation of the solidifying cementitious material by the dissolution of siliceous aggregate. The present study demonstrates that geochemical modelling by using the Gibbs Energy Minimization Selektor (GEM-Selektor) software package allows the long-term evolution of the chemical conditions in waste forms to be assessed for different design options, for example the replacement of siliceous by calcareous aggregate for fabrication of the solidifying cementitious material. The results suggest that adequate knowledge of internal degradation processes in waste forms provides supporting information in connection with an overall assessment of the long-term safety of an L/ILW repository. For example, using calcareous aggregate instead of siliceous aggregate for fabrication of the solidifying cementitious material allows highly alkaline conditions in the waste form to be maintained over the period of concern for the L/ILW repository.

Geochemical modelling further shows that water plays a decisive role in waste degradation. All the aforementioned degradation processes are water-consuming reactions except carbonation, which releases water. In the absence of water ingress from the near field, the degradation processes come to a halt once free water in the waste package is exhausted. In a saturated system achieved by water ingress, however, the degradation processes continue over the entire period of concern for the L/ILW repository.

The geochemical modelling approach reported in this study provides a tool for an overall assessment of the relevance and consequences of the individual chemical processes that govern the chemical evolution of a waste form. Various initial conditions and model assumptions can be

considered, such as varying waste inventories and varying compositions of the solidifying (conditioning) cementitious material, as it has been demonstrated for the model waste form used in the present case study. Thus, it is believed that the proposed modelling approach is well suited for "screening" applications, while it is of limited use for realistic predictions of the long-term evolution of waste forms in time and space. In particular, the approach does not provide information on the spatially resolved evolution of the chemical conditions in a waste package, as it is based on the concept of a "mixing tank". Furthermore, the current approach does not account for the effect of gas production on transport processes in the waste package, which requires new developments in the framework of coupled two-phase reactive transport modelling (e.g. Huang et al., 2018).

Acknowledgement

Partial financial support was provided by the National Cooperative for the Disposal of Radioactive Waste (Nagra), Switzerland.

Disclaimer

The views, opinions and conclusions of the authors herein do not necessarily state or reflect those of Nagra. The kinetic parameters, materials and inventories used in this study are not necessarily those of the reference concept of Nagra and future license applications.

References

Askarieh, M.M., Chambers, A.V., Kickford, G.E., Sharland, S.M., 1998. The role of engineered barriers in the performance assessment of a repository for L/ILW. Mat. Res. Soc. Symp. Proc. 506, 465-476.

Askarieh, M.M., Chambers, A.V., Gould, L.J., 2000. Research into the effects of repository heterogeneity. Mat. Res. Soc. Symp. Proc. 608, 243-248.

Bach, T.T.H., Chabas, E., Pochard, I., Cau Dit Coumes, C., Haas, J., Frizon, F., Nonat, A., 2013. Retention of alkali ions by hydrated low-pH cements: Mechanism and Na^+/K^+ selectivity. Cem. Concr. Res. 51, 14-21.

Berner, U., 2009. Modelling hydrated HTS cement and its pore water, PSI Internal Report AN-44-09-10, Paul Scherrer Institut, Villigen PSI, Switzerland.

Bérubé, M.A., Fournier, B., Durand, B. (eds), 2000. Alkali-aggregate reaction in concrete. Proceedings of the 11th International Conference on Alkali-Aggregate Reaction in Concrete, CRIB, Sainte Foy, Québec City, Canada.

Blanc, P., Vieillard, P., Gailhanou, H., Gaboreau, S., Marty, N., Claret, F., Madé, B., Giffault, E., 2012. Thermoddem: A geochemical database focused on low temperature water/rock interactions and waste materials. Appl. Geochem. 27, 2107-2116.

Cau Dit Coumes, C., Courtois, S., Nectoux, D., Leclerq, S., Bourbon, X., 2006. Formulating a low-alkalinity, high-resistance and low-heat cementitious material for radioactive waste repositories. Cem. Concr. Res. 36, 2152-2163.

Cochepin, B. Trotignong, L., Bildstein, O., Steefel, C.I., Lagneau, V., Van der Lee, J., 2008. Approaches to modelling coupled flow and reaction in a 2D cementation experiment. Adv. Water Resour. 31, 1540-1551.

De Windt, L., Pellegrini, D., van der Lee, J., 2004. Coupled modeling of cement/claystone interactions and radionuclide migration. J. Contam. Hydrol. 68, 165-182.

Diomidis, N., 2014. Scientific basis for the production of gas due to corrosion in a deep geological repository. Nagra Work Report NAB 14-21, Nagra, Wettingen, Switzerland.

Diomidis, N., Cloet, V., Leupin, O.X., Marschall, P., Poller, A., Stein, M., 2016. Production, consumption and transport of gases in deep geological repositories according to the Swiss disposal concept. Nagra Technical Report NTB 16-03, Nagra, Wettingen, Switzerland.

Garcia Calvo, J.L., Hidalgo, A., Alonso, C., Fernandez Luco, L., 2010. Development of low-pH cementitious materials for HLRW repositories. Resistance against ground waters aggression. Cem. Concr. Res. 40, 1290-1297.

Gaucher, E.C., Blanc, P., Matray, J.-M., Michau, N., 2004. Modeling diffusion of an alkaline plume in a clay barrier. Appl. Geochem. 19, 1505-1515.

Gruskovnjak, A., Lothenbach, B., Winnefeld, F., Münch, B., Ko, S.C., Adler, M., Mäder, U., 2011. Quantification of hydration phases in super sulphated cements: Review and new approaches. Adv. Cem. Res. 23, 265-275.

Helgeson, H., Delany, J., Nesbitt, H., Bird, D., 1978. Summary and critique of the thermodynamic properties of rock-forming minerals. Am. J. Sci. 278, 1-229.

Hong, S.-Y., Glasser, F.P., 1999. Alkali binding in cement pastes - Part I. The C-S-H phase. Cem. Concr. Res. 29, 1893-1903.

Huang, Y., Shao, H., Wieland, E., Kolditz, O., Kosakowski, G., 2018. A new approach to coupled two-phase reactive transport simulation for long-term degradation of cementitious material. Constr. Build. Mater. 190, 805-829.

Hummel, W., Berner, U., Curti, E., Pearson, F.J., Thoenen, T., 2002. Nagra/PSI chemical thermodynamic data base 01/01, Universal Publishers/uPUBLISH.com, USA, also published as Nagra Technical Report NTB 02-16, Nagra, Wettingen, Switzerland, 2002.

Johnson, J., Oelkers, E., Helgeson, H., 1992. SUPCRT92 - A software package for calculating the standard molal thermodynamic properties of minerals, gases, aqueous species, and reactions from 1 bar to 5000 bar and 0 degrees-C to 1000-degrees-C. Comput. Geosci. 18, 899-947.

Kannen, H., Müller, W., 1999. Gas generation of radioactive waste - Comparison between laboratory experiments and measurements on real waste. Radioactive Waste Management and Environmental Remediation. ICEM Conference Proceedings. ASME, Nagoya, Japan.

Kosakowski, G., Berner, U., 2013. The evolution of clay rock/cement interfaces in a cementitious repository for low- and intermediate level radioactive waste. Phys. Chem. Earth 64, 65-86.

Kosakowski, G., Berner, U., Wieland, E., Glaus, M., Degueldre, C., 2014. Geochemical evolution of the L/ILW near field. Nagra Technical Report NTB 14-11, Nagra, Wettingen, Switzerland.

Kulik, D.A., Tits, J., Wieland, E., 2007. Aqueous-solid solution model of strontium uptake in C-S-H phases. Geochim. Cosmochim. Acta 71, A530.

Kulik, D.A., Wagner, T., Dmytrieva, S.V., Kosakowski, G., Hingerl, F.F., Chudnenko, K.V., Berner, U., 2013. GEM-Selektor geochemical modeling package: revised algorithm and GEMS3K numerical kernel for coupled simulation codes. Computat. Geosci. 17, 1-24.

Lagerblad, B., 2005. Carbon dioxide uptake during concrete life cycle: State of the Art, CBI Report 2:2005, Swedish Cement and Concrete Research Institute, Stockholm, Sweden.

Leupin, O.X, Zeyer, J., Cloet, V., Smith, P., Bernier-Latmani, R., Marschall, P., Papafotiou, A., Schwyn, B., Stroes-Gascoyne, S., 2016. An assessment of the possible fate of gas generated in a repository for low- and intermediate-level waste. Nagra Technical Report NTB 16-05, Nagra, Wettingen, Switzerland.

L'Hôpital, E., Lothenbach, B., Scrivener, K., Kulik, D.A., 2016. Alkali uptake in calcium alumina silicate hydrate (CASH), Cem. Concr. Res. 85, 122–136.

Lothenbach, B., Wieland, E., 2006. A thermodynamic approach to the hydration of sulphate-resisting Portland cement. Waste Manage. 26, 706-719.

Lothenbach, B., Gruskovnjak, A., 2007. Hydration of alkali-activated slag: thermodynamic modelling. Adv. Cem. Res. 19, 81-92.

Lothenbach, B., Le Saout, G., Ben Haha, M., Figi, R., Wieland, E., 2012a. Hydration of a low-alkali CEM III/B-SiO_2 cement (LAC). Cem. Concr. Res. 42, 410-423.

Lothenbach, B., Pelletier-Chaignat, L., Winnefeld, F., 2012b. Stability in the system $CaO-Al_2O_3-H_2O$. Cem. Concr. Res. 42, 1621-1634.

Lothenbach, B., Rentsch, D., Wieland, E., 2014. Hydration of a silica fume blended low-alkali shotcrete cement. Phys. Chem. Earth 70-71, 3-16.

Lothenbach, B., Bernard, E., Mäder, U., 2017. Zeolite formation in the presence of cement hydrates and albite. Phys. Chem. Earth 99, 77-94.

Lothenbach, B., Kulik, D.A., Matschei, T., Balonis, M., Baquerizo, L., Dilnesa, B., Miron, G.D., Myers, R.J., 2019. Cemdata18: A chemical thermodynamic database for hydrated Portland cements and alkali-activated materials. Cem. Concr. Res. 115, 472-506.

Marty, N.C.M., Bildstein, O., Blanc, Ph., Claret, F., Cochepin, B., Gaucher, E.C., Jacques, D., Lartigue, J-E., Liu, S., Mayer, U., Meeussen, J.C.L., Munier, I., Pointeau, I., Su, D., Steefel, C.I., 2015. Benchmarks for multicomponent reactive transport across a cement/clay interface. Computat. Geosci. 19, 635-653.

Nagra, 2002. Project Opalinus Clay: Models, codes and data for safety assessment. Demonstration of disposal feasibility for spent fuel, vitrified high-level waste and long-lived intermediate-level waste (Entsorgungsnachweis). Nagra Technical Report NTB 02-05, Nagra, Wettingen, Switzerland.

Nagra, 2008. Effects of post-disposal gas generation in a repository for low- and intermediate-level waste sited in the Opalinus Clay of Northern Switzerland. Nagra Technical Report NTB 08-07, Nagra, Wettingen, Switzerland.

Nagra, 2014. Modellhaftes Inventar für radioaktive Materialien MIRAM 14. Nagra Technical Report NTB 14-04, Nagra, Wettingen, Switzerland.

Nagra, 2016. Waste management programme 2016 of the waste producers. Nagra Technical Report NTB 16-01E, Nagra, Wettingen, Switzerland.

Palandri, J.L., Kharaka, Y.K., 2004. A compilation of rate parameters of water-mineral interaction kinetics for application to geochemical modeling. Open File Report 2004-2008, U.S. Geological Survey, Menlo Park, California.

Poller, A., Mayer, G., Darcis, M., Smith, P., 2016. Modelling of gas generation in deep geological repositories after closure. Nagra Technical Report NTB 16-04, Nagra, Wettingen, Switzerland.

Robie, R.A., Hemingway, B.S., 1995. Thermodynamic properties of minerals and related substances at 298.15 K and 1 bar (10^5 Pascals) pressure and at higher temperatures. US Geological Survey Bulletin 2131.

Rossen, J.E., Lothenbach, B., Scrivener, K.L., 2015. Composition of C-S-H in pastes with increasing level of silica fume addition. Cem. Concr. Res. 75, 14-22.

836 Small, J.S., Nykyri, M., Paaso, N., Hovi, U., Itävaara, M., Sarlin, T., 2006. Testing of a near-field
837 biogeochemical model against data from a large-scale gas generation experiment. Mat.
838 Res. Soc. Symp. Proc. 932, 111-118.

839 Small, J.S., Thompson, O.R., 2008. Development of a model of the spatial and temporal evolution
840 of pH in cementitious backfill of a geological disposal facility. Nuclear National Laboratory
841 Report NNL(08) 9601 Issue 4.

842 Small, J.S., Nykyri, M., Helin, M., Hovi, U., Sarlin, T., Itävaara, M., 2008. Experimental and
843 modelling investigations of the biogeochemistry of gas production from low and
844 intermediate level radioactive waste. Appl. Geochem. 23, 1383-1418.

845 Small, J.S., Nykyri, M., Vikman, M., Itävaara, M., Heikinheimo, L., 2017. The biogeochemistry of gas
846 generation from low-level nuclear waste: Modelling after 18 years study under *in situ*
847 conditions. Appl. Geochem. 84, 360-372.

848 Sullivan, T., 2004. Waste container and waste package performance: Modeling to support safety
849 assessment of low- and intermediate-level radioactive waste disposal. Report BNL-74700-
850 2005-IR, Brookhaven National Laboratory, Upton, New York, USA.

851 Thoenen, T., Hummel, W., Berner, U., Curti, E., 2014. The PSI/Nagra chemical thermodynamic
852 database 12/07. PSI Report 14-04, Paul Scherrer Institut, Villigen PSI, Switzerland.

853 Walton, J.C., BinShafique, S., Smith, R.W., Gutierrez, N., Tarquin, A., 1997. Role of carbonation in
854 transient leaching of cementitious wasteforms. Environ. Sci. Technol. 31, 2345-2349.

855 Warthmann, R., Mosberger, L., Baier, U., 2013. Langzeit-Degradation von organischen Polymeren
856 unter SMA-Tiefenlagerbedingungen. Nagra Technical Report NTB 13-04, Nagra, Wettingen,
857 Switzerland.

858 Wiborgh, M., Höglund, L.O., Pers, K., 1986. Gas formation in a L/ILW repository and gas transport
859 in the host rock. Nagra Technical Report NTB 85-17, Nagra, Wettingen, Switzerland.

860 Wieland, E., Kosakowski, G., Lothenbach, B., Kulik, D.A., Cloet, V., 2018. Preliminary assessment of
861 the temporal evolution of waste packages in the near field of the L/ILW repository. Nagra
862 Work Report NAB 18-05, Nagra, Wettingen, Switzerland.

863 Wieland, E., 2019. Geochemical modelling of the temporal evolution of L/ILW waste sorts with
864 siliceous and calcareous aggegates. PSI Technical Report TM-44-19-08, Paul Scherrer
865 Institut, Villigen PSI, Switzerland.

866

Highlights

- Geochemical modelling allows prediction of the chemical evolution of waste forms
- The model waste form consists of waste materials conditioned in a cementitious matrix
- Degradation of waste and dissolution of aggregate determine the chemical evolution
- The type of aggregate has a strong effect on the chemical evolution
- Calcareous aggregates maintain the strongly alkaline conditions in the waste form

Declaration of interests

☒ The authors declare that they have no known competing financial interests or personal relationships that could have appeared to influence the work reported in this paper.

☐The authors declare the following financial interests/personal relationships which may be considered as potential competing interests: